RSC Advances

PAPER

View Article Online
View Journal | View Issue

Cite this: *RSC Adv.*, 2019, **9**, 2018

Synthesis and photocatalytic activities of a CuO/TiO_2 composite catalyst using aquatic plants with accumulated copper as a template

Dongfang Lu,[a] Osman Ahmed Zelekew,[b] Angaw Kelemework Abay,[c] Qitang Huang,[a] Xiaoyun Chen*[d] and Yushan Zheng*[a]

A CuO/TiO_2 composite photocatalyst was synthesized by using a hydrolysis method. In the synthesis of the CuO/TiO_2 composite catalyst, the aquatic plant *Eichhornia crassipes* containing accumulated copper was used and combined with titanium chloride precursor. X-ray diffraction (XRD), X-ray photoelectron spectroscopy (XPS), scanning electron microscopy (SEM), transmission electron microscopy (TEM), UV-Vis diffuse spectroscopy (DRS), and N_2 adsorption–desorption isotherms were used for CuO/TiO_2 characterization. The results showed that the CuO/TiO_2 synthesized with *Eichhornia crassipes* as a template had smaller crystallite size (12.6 nm), higher specific surface area (109 m^2 g^{-1}), and higher pore volume (0.135 cm^3 g^{-1}). The catalytic activity of the CuO/TiO_2 composite catalyst was also investigated by the degradation of phenol under ultraviolet (UV) and visible light irradiation, showing excellent catalytic activity. Complete removal of phenol was achieved at 80 and 120 min under UV and visible light sources, respectively. The catalytic performances may be due to the higher porosity and surface area of the composite catalyst. The *Eichhornia crassipes* aquatic plant also controls the crystal growth and prevents aggregation, which could enhance the catalytic activity. Moreover, the formation of the p–n CuO/TiO_2 heterojunction also facilitates the separation of electrons and holes, and improves the photocatalytic activity of the material.

Received 23rd November 2018
Accepted 21st December 2018

DOI: 10.1039/c8ra09645g

rsc.li/rsc-advances

1. Introduction

Nowadays, the energy crisis and environmental pollution problems are current and global issues, and significant attention has been given to solving these problems by different methods.[1–5] The application of suitable semiconductor materials for hydrogen production, CO_2 reduction, pollutant degradation, and solar cells is also a current issue for scientists.[6–10] In particular, treatment of industrial wastewater containing toxic heavy metals and aromatic organic pollutants has become a very big challenge for researchers.[11–13] For this reason, researchers have tried to decontaminate wastewaters with the aid of different techniques, such as photocatalysis, biological, and other conventional methods.[14–18] Among the techniques used, photocatalysis is a powerful method for the decontamination of wastewaters.[19,20] The photocatalytic degradation of pollutants by using high performance semiconductor catalysts has been also confirmed as one of the most promising strategies to clean the environment.[21]

Currently, the remediation of environmental pollution is focused on using metal oxide based photocatalysts, and TiO_2 has become a promising metal oxide photocatalytic material because of its stability and catalytic efficiency.[22,23] However, the photocatalytic activities with TiO_2 catalysts is typically suitable under UV irradiation owing to the large band gap energy (3.2 eV), and this limits TiO_2 in practical applications.[22–24] For this reason, researchers have tried to modify the TiO_2 semiconductor material to be active in the visible region of the electromagnetic spectrum for different applications.[25,26] Among the methods used for making TiO_2 semiconductors active under visible light are doping, combination of TiO_2 with other lower band gap metal oxides and others.[27–29] In addition to doping or combination of TiO_2 with other materials, the application of porous metal oxides has also many advantages in the remediation of environmental pollution.[30,31] Reports have also shown that synthesized mesoporous TiO_2 exhibits a high specific surface area and enhances the catalytic activity.[32,33] For this purpose, biological renewable resources such as lignin and cellulose templates for the preparation of mesoporous metal oxide materials are significantly important for wastewater treatment, as reported by different researchers.[34–36] Also, bio-template methods for the synthesis of materials for the

[a]*College of Landscape Architecture, Fujian Agriculture & Forestry University, Fuzhou 350002, China. E-mail: yszheng@126.com*

[b]*Department of Materials Science and Engineering, Adama Science and Technology University, Adama, Ethiopia*

[c]*Department of Chemistry, College of Science, Jigjiga University, Jigjiga, Ethiopia*

[d]*College of Material Engineering, Fujian Agriculture & Forestry University, Fuzhou 350002, China. E-mail: fjchenxy@126.com*

decontamination of wastewater are believed to be green and environment-friendly and so are favored by the scientific community.[37–39]

Recently, Chen *et al.* synthesized mesoporous TiO_2 nanoparticles using the biological renewable resource unmodified lignin and N-doped mesoporous TiO_2 nanoparticles with biological renewable nanocrystalline cellulose as template for photocatalytic degradation of pollutants.[40,41] Zhou *et al.* synthesized TiO_2 nanocubes induced by cellulose nanocrystals (CNCs) at low temperature.[42] Moreover, Miao *et al.* prepared mesoporous TiO_2 films using titanium tetrabutyloxide and cellulose.[43] TiO_2 immobilized on carbon materials derived from renewable and biodegradable resources and morph-TiO_2 from green-leaf biotemplates have also been synthesized to enhance photocatalytic activity.[34,44] However, utilization of the aquatic plant *Eichhornia crassipes* containing accumulated copper combined with TiO_2 has not previously been reported.

In this paper, a CuO/TiO_2 composite photocatalyst was prepared by a simple and green method using *Eichhornia crassipes* aquatic plant containing accumulated copper as a template. The effects of the *Eichhornia crassipes* template on the catalytic activity were studied systematically. Moreover, TiO_2-Tep with the *Eichhornia crassipes* and without copper aqueous solution, and TiO_2 without using the *Eichhornia crassipes* template were also prepared and used for comparison purposes. Commercially available P25-TiO_2 was also compared with the synthesized composite catalyst. To investigate the catalytic activities of the materials under UV and visible light sources, phenol was used as pollutant. Hence, the synthesis of combined p-type CuO semiconductor from copper-enriched *Eichhornia crassipes* and n-type TiO_2 semiconductor is expected to enhance the photocatalytic degradation of phenol under UV and visible light sources.

2. Experimental methods

2.1. Chemicals

All chemicals in this experiment were analytical grade and used without further purifications.

2.2. Preparation of template

In this experiment, the aquatic plant *Eichhornia crassipes* was used as a template. The plant was used after it had been immersed in 20 mg L^{-1} copper nitrate solution for one week. Then, the *Eichhornia crassipes*, which had accumulated copper, was dried and crushed to a particle size of about 100–120 mesh. Finally, the resulting crushed samples were collected and stored for further use.

2.3. Catalyst preparation

The composite catalyst was prepared with a simple and green method. In this particular procedure, 10 ml of $TiCl_4$ was added dropwise into 200 ml solution containing 1 g L^{-1} *Eichhornia crassipes* with accumulated copper and stirred for 30 min. Subsequently, the solution was heated at 80 °C under continuous stirring. After stirring for 30 min, $NH_3 \cdot H_2O$ was added dropwise into the solution in order to adjust the pH to 7. After stirring for another 30 min, the precipitate was aged for 10 h at room temperature. The resulting precipitate was washed with distilled water and anhydrous ethanol. Finally, the product was dried at 85 °C under vacuum for 24 h, and calcined at 500 °C for 2 h in air. Then, the CuO/TiO_2 composite catalyst was obtained. For comparison purposes, TiO_2-Tep made with *Eichhornia crassipes* and without copper aqueous solution, and TiO_2 without using the *Eichhornia crassipes* template were prepared by similar procedures. Commercially available P25-TiO_2 was also used for comparison in this experiment.

2.4. Characterizations

An X-ray diffraction (XRD) system (Rigaku diffractometer with Cu Kα radiation source) was used to examine the crystal structure of the photocatalytic composite material. Transmission electron microscopy (TEM, Tecnai G2 F20) with an accelerating voltage of 200 kV was used to observe the microstructure of the catalysts. X-ray photoelectron spectrometry measurement was conducted by means of a Physical Electronics PHI5700 photoelectron spectrometer with Al Kα ($h\nu$ = 1486.6 eV) radiation source. The ultraviolet–visible diffuse reflectance spectra measurements were recorded using a TU-1901 UV-Vis spectrophotometer. N_2 adsorption–desorption experiments were also performed using a SSA4300 analyzer after degassing for 2 h at 200 °C.

2.5. Catalyst activity measurements

The performance of the composite catalyst was tested in a home-made jacketed quartz reactor. A mercury lamp (8 W) was used as a source of UV light. A Xe lamp (350 W) with wavelength filtered to below 400 nm was used as a source of visible light. We used 250 ml of phenol solution (50 mg L^{-1}) for the photocatalytic degradation test. In the reaction mixture, 0.125 g of the catalyst was used and the mixture was stirred for 30 min in the dark to obtain adsorption–desorption equilibrium. Air flow was supplied into the reactor throughout the reaction. Finally, a 5 ml aliquot of solution was taken out at intervals of 20 min from the reactor and centrifuged. Then, the supernatant was examined by using a TU-1901 UV-Vis spectrophotometer and concentration was calculated by means of the Lambert–Beer law.

3. Results and discussion

3.1. XRD analysis

The XRD diffraction patterns of the CuO/TiO_2 composite, TiO_2-Tep, and TiO_2 annealed at 500 °C are shown in Fig. 1. As we see from Fig. 1, the characteristic peak positions of anatase and rutile at 25.27° and 27.48°, respectively, were not affected by the *Eichhornia crassipes* template. However, the amounts of rutile formed in the CuO/TiO_2 composite and TiO_2-Tep were smaller as compared with the template-free TiO_2 after calcination at 500 °C. Thus, the transition from anatase to rutile was controlled by the *Eichhornia crassipes* template and the change was relatively difficult. Moreover, the average crystallite sizes of

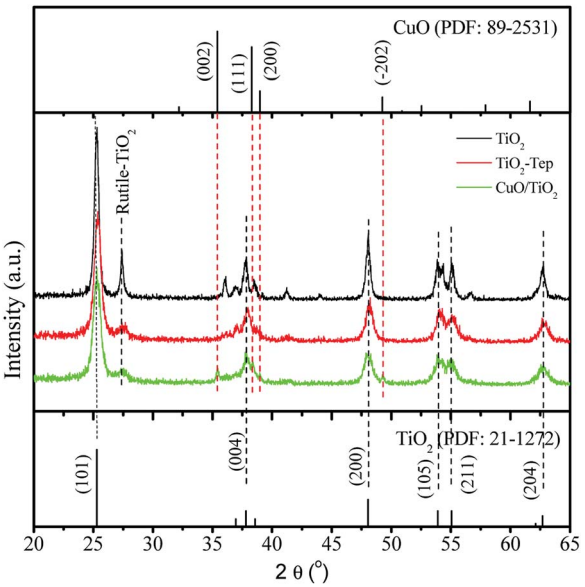

Fig. 1 XRD pattern of CuO/TiO_2, TiO_2-Tep, and TiO_2 catalysts.

the catalysts calculated by means of the Scherrer formula are listed in Table 1. As we see from Table 1, the crystallite sizes of the CuO/TiO_2 and TiO_2-Tep were 12.6 and 12.3 nm, respectively. However, the crystallite size of the template-free TiO_2 was 18.1 nm. This shows that the use of the *Eichhornia crassipes* template in the synthesis TiO_2 nanoparticles made the crystallite size smaller. The smaller crystallite size may be due to the three-dimensional network of *Eichhornia crassipes* blocking the crystal growth. On the other hand, the functional groups on the surface of the *Eichhornia crassipes* template may bond with hydroxides of Ti which could limit agglomeration and inhibit the TiO_2 transition from anatase to rutile.[45] In addition to this, a smaller peak was also observed at about 35.4° due to the presence of CuO in the composite catalyst.

3.2. XPS analysis

Fig. 2 shows the XPS spectra for the CuO/TiO_2 composite and for TiO_2 made without using the template. As we see from Fig. 2a, the high resolution Ti2p XPS spectra of CuO/TiO_2 and TiO_2, contain peaks located at 458.3 and 464.2 eV belonging to $Ti2p_{3/2}$ and $Ti2p_{1/2}$, respectively, of Ti^{4+}. Fig. 2b shows the high resolution O1s XPS spectra of CuO/TiO_2 and TiO_2. The peaks at 529.6 and 531.3 eV belong to the lattice oxygen and the hydroxyl oxygen, respectively. Moreover, Fig. 2c shows the Cu2p XPS spectrum of the CuO/TiO_2 composite catalyst. The peaks at 934.6 and 954.5 eV belong to $Cu2p_{3/2}$ and $Cu2p_{1/2}$, respectively, which indicates the formation of Cu^{2+} in the composite.[46,47] The peaks at 944.2 eV and 963.8 eV are the satellite peaks for Cu^{2+}. As we have seen from the results, the XPS and the XRD data further confirmed the formation of CuO in the composite.

3.3. N_2 adsorption–desorption isotherm analysis

The N_2 adsorption–desorption isotherms of the CuO/TiO_2 composite and TiO_2 catalysts prepared at 500 °C are shown in Fig. 3a. The results show hysteresis loops and the type IV adsorption–desorption isotherm. It is known that a hysteresis loop indicates the presence of mesoporous structure in the catalyst.[48] Fig. 3b displays the pore size distribution curve. A pore diameter of 1–11 nm and a total pore volume of 0.135 $cm^3\ g^{-1}$ were obtained for the CuO/TiO_2 prepared with the *Eichhornia crassipes* template. However, 1–30 nm pore diameter and 0.0159 $cm^3\ g^{-1}$ total pore volume were obtained for the TiO_2 prepared without template. Furthermore, the specific surface areas of the samples were calculated according to the BET equation and are shown in Table 1. The S_{BET} for CuO/TiO_2 was 109 $m^2\ g^{-1}$, which was higher than that of 43.8 $m^2\ g^{-1}$ for TiO_2. This indicates that the utilization of the *Eichhornia crassipes* template was advantageous for narrowing pore size distribution and increasing pore volume and specific surface area. This may be due to the decomposition of the *Eichhornia crassipes* template at high temperature and attributed to the formation of a porous networked structure in the TiO_2 particles.

3.4. SEM and TEM analysis

The SEM and TEM images of TiO_2 and CuO/TiO_2 are shown in Fig. 4a–e. As we see from the SEM (Fig. 4a) and TEM (Fig. 4c) images, the TiO_2 prepared without template contained larger aggregated particles. However, the CuO/TiO_2 composite catalyst prepared in the presence of *Eichhornia crassipes* template had smaller aggregates with a particle size of 30–100 nm (Fig. 4b). In the TEM image (Fig. 4d), we observe several pores measuring 2–10 nm and well distributed CuO/TiO_2 particles. However, there was no porosity in the TiO_2 particle prepared without *Eichhornia crassipes* (Fig. 4b). It is known that the presence of many uniform nanopores is advantageous because it enhances the surface permeability and improves its adsorption performance. It also enables the rapid transfer of light-excited carriers to the particle surface, to effectively reduce the carrier recombination rate and accelerate photocatalytic reactions.[49] Fig. 4e shows the HR-TEM image of CuO/TiO_2. The *d*-spacing value of TiO_2 was 3.52 Å for the (101) plane, and the d-spacing value of CuO was

Table 1 Crystallite size and surface area of catalysts, and the kinetic parameters of phenol photocatalytic degradation[a]

Sample	Crystallite size/nm	$S_{BET}/(m^2\ g^{-1})$	Phenol removal[b]/%	k/min^{-1}	R^2
CuO/TiO_2	12.6	109	100	0.1405	0.8782
TiO_2-Tep	12.3	112	77.3	0.0694	0.8756
TiO_2	18.1	43.8	55.8	0.0323	0.9395
P25-TiO_2	21.0	50.0	64.1	0.0676	0.8898

[a] *k*, reaction constant. [b] At 80 min.

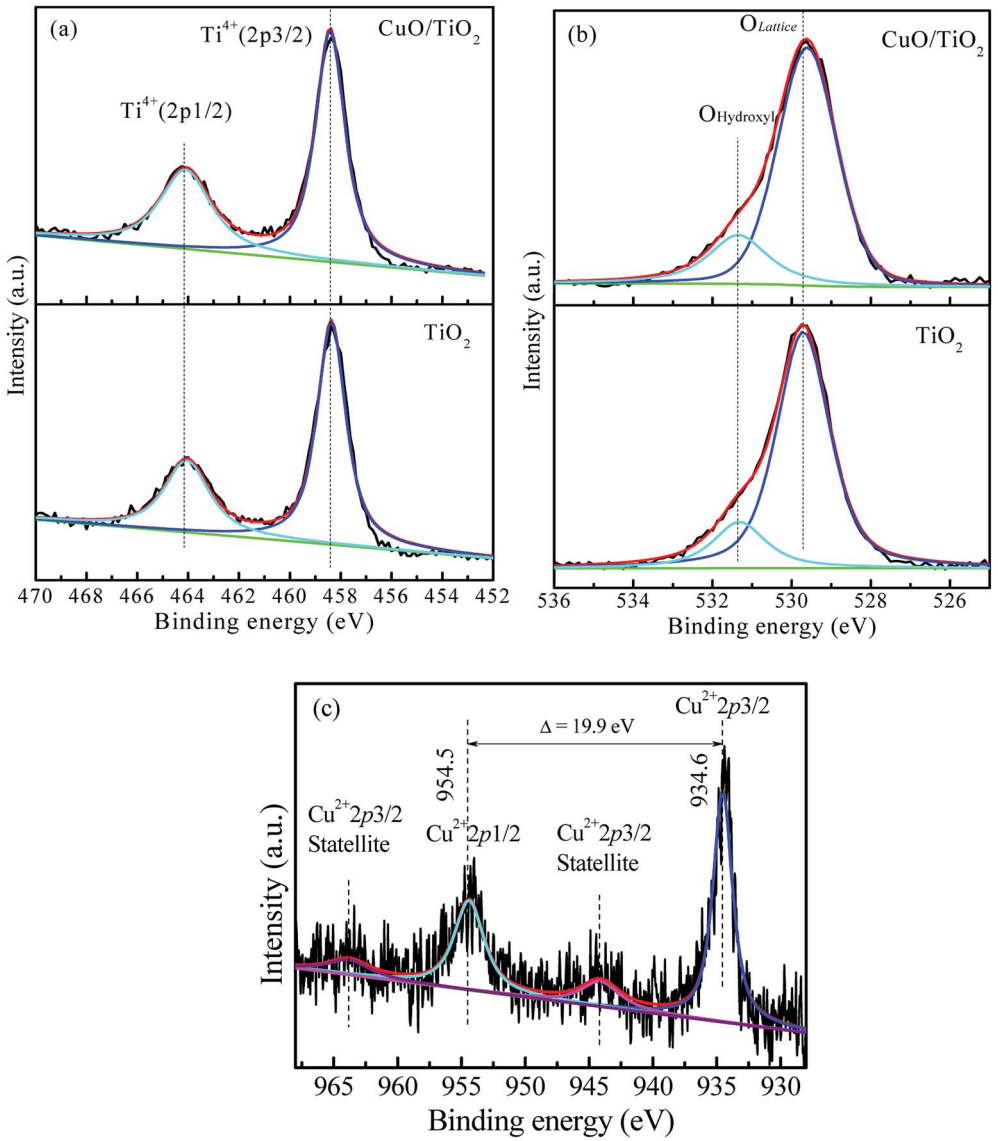

Fig. 2 XPS spectra of (a) Ti2p and (b) O1s for CuO/TiO_2 and TiO_2 catalysts. (c) Cu2p for the CuO/TiO_2 catalyst.

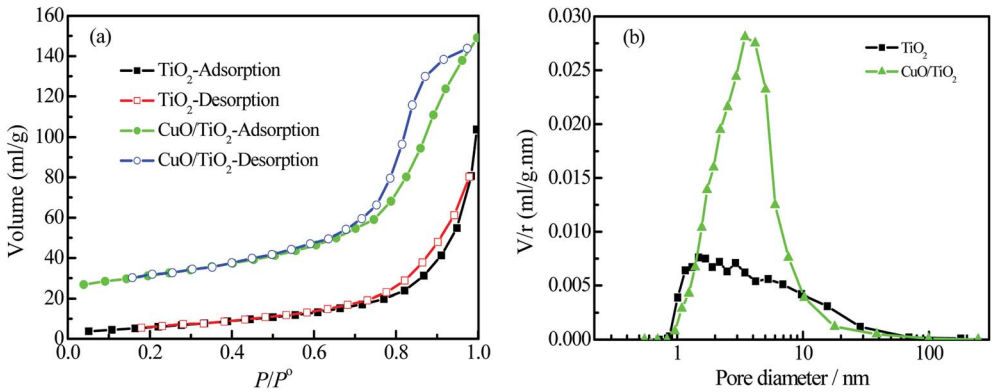

Fig. 3 (a) Nitrogen adsorption–desorption isotherms and (b) pore size distribution curves of CuO/TiO_2 and TiO_2.

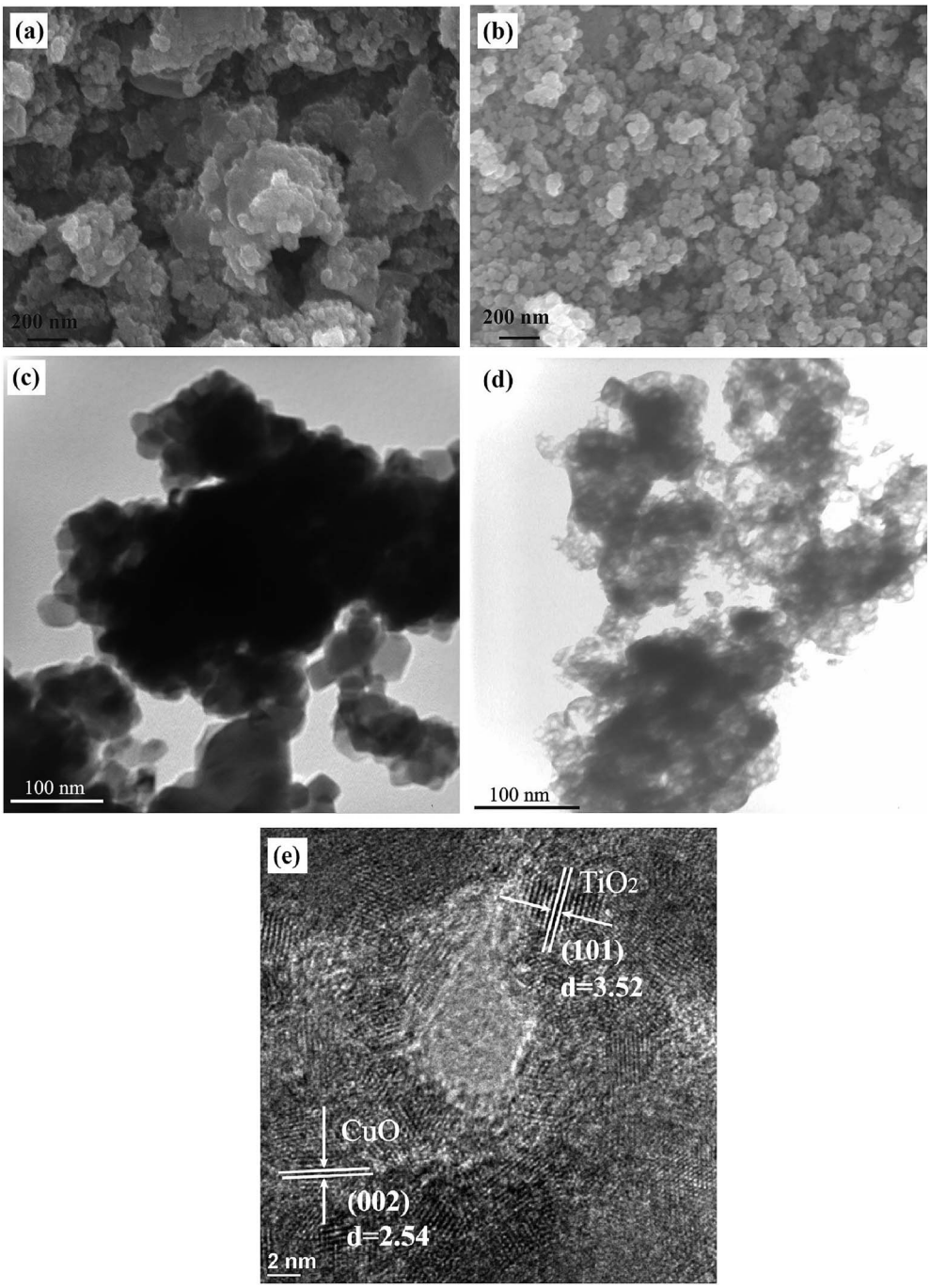

Fig. 4 SEM images of (a) TiO_2 and (b) CuO/TiO_2, TEM images of (c) TiO_2 and (d) CuO/TiO_2, and HR-TEM image (e) of CuO/TiO_2 catalyst.

2.540 Å for the (002) plane. These results further confirm the presence of CuO and TiO_2 particles in the composite catalyst.

3.5. UV-Vis diffuse reflectance spectrum analysis

The UV-Vis diffuse reflectance spectrum (DRS) spectra of the CuO/TiO_2, TiO_2-Tep and TiO_2 catalysts are shown in Fig. 5. It can be seen that the copper-free *Eichhornia crassipes* template had no effect on the absorption threshold of TiO_2, and the light in the ultraviolet and visible light regions. However, CuO/TiO_2 synthesized with Cu-enriched *Eichhornia crassipes* template significantly increased the absorption in the visible region, owing to the absorption of light by CuO nanoparticles. But, the TiO_2 had no influence in the ultraviolet light region and on the light absorption threshold of the lattice structure. It is suggested that the combination of n-type semiconductor with p-type semiconductor creates an internal electric field and causes the formation of a p–n heterojunction. The formation of this p–n heterojunction and the band alignment between CuO and TiO_2 also greatly facilitate the electron–hole separation and enhance the catalytic activity.[32,50]

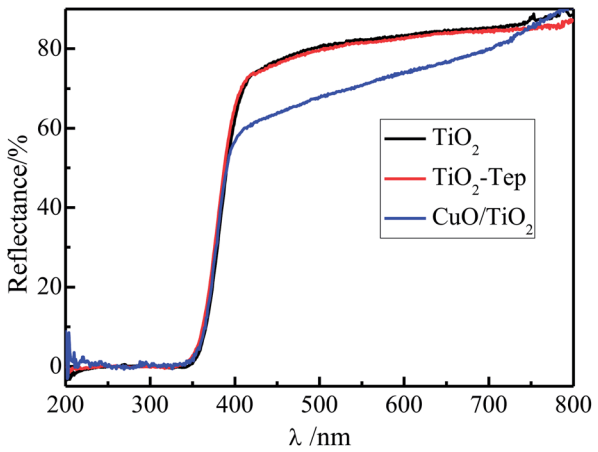

Fig. 5 Diffuse reflectance spectra of CuO/TiO_2, TiO_2-Tep, and TiO_2 catalysts.

3.6. Photocatalytic activity

Fig. 6a shows the catalytic activities of the CuO/TiO_2, TiO_2-Tep, TiO_2, and P25-TiO_2 under UV light irradiation. It was observed that the catalytic activity of the CuO/TiO_2 was significantly higher than those of the TiO_2-Tep, TiO_2, and P25-TiO_2. Phenol was completely removed by CuO/TiO_2 in 80 min. However, phenol removal by TiO_2-Tep, TiO_2, and P25-TiO_2 reached 100%, 82.6%, and 91.4%, respectively, in 140 min. Based on the kinetic analysis, the phenol photocatalytic degradation reaction was also well fitted with pseudo-first-order kinetics. The first-order reaction rate constant (k) sequence was CuO/TiO_2 (k = 0.1405 min^{-1}) > TiO_2-Tep (k = 0.06942 min^{-1}) > P25-TiO_2 (k = 0.06756 min^{-1}) > TiO_2 (k = 0.03232 min^{-1}). Fig. 6b shows the activities of the different catalysts under visible light. It is obvious that CuO/TiO_2 completely removed phenol in 120 min, but only 19.6%, 8.1%, and 11.3% was removed by TiO_2-Tep, TiO_2, and P25-TiO_2, respectively. In order to test the CuO/TiO_2 capability and reusability, the CuO/TiO_2 catalyst was continuously tested for six runs under visible light, with the results shown in Fig. 6c. The CuO/TiO_2 composite catalyst proved to be stable, retaining good degradation activity for removal of phenol of about 92.5% on the 6th run.

The improvement of catalytic efficiency of the CuO/TiO_2 could be due to the combination of p-type CuO and n-type TiO_2 semiconductors. When p-type and n-type semiconductors combine together, a p–n heterojunction is formed. Owing to the presence of carrier concentration gradients, photogenerated holes diffuse from p-type to n-type region and electrons diffuse from n-type to p-type region. At equilibrium, an electric field is created at the junction.[51,52] During photocatalysis, the photogenerated electrons can move to the conduction band of the n-type TiO_2 and holes can move to the valence band of the p-type CuO. The p–n CuO/TiO_2 heterojunction formation facilitates the separation of photogenerated electrons and holes and improves the photocatalytic activities of the materials.[29] For this reason, the CuO/TiO_2 catalyst had higher photocatalytic activity than TiO_2-Tep, TiO_2, and P25-TiO_2.

3.7. Mechanism for *Eichhornia crassipes* template synthesis of TiO_2

The aquatic plant *Eichhornia crassipes* has a natural three-dimensional network structure with many hydroxyl groups.

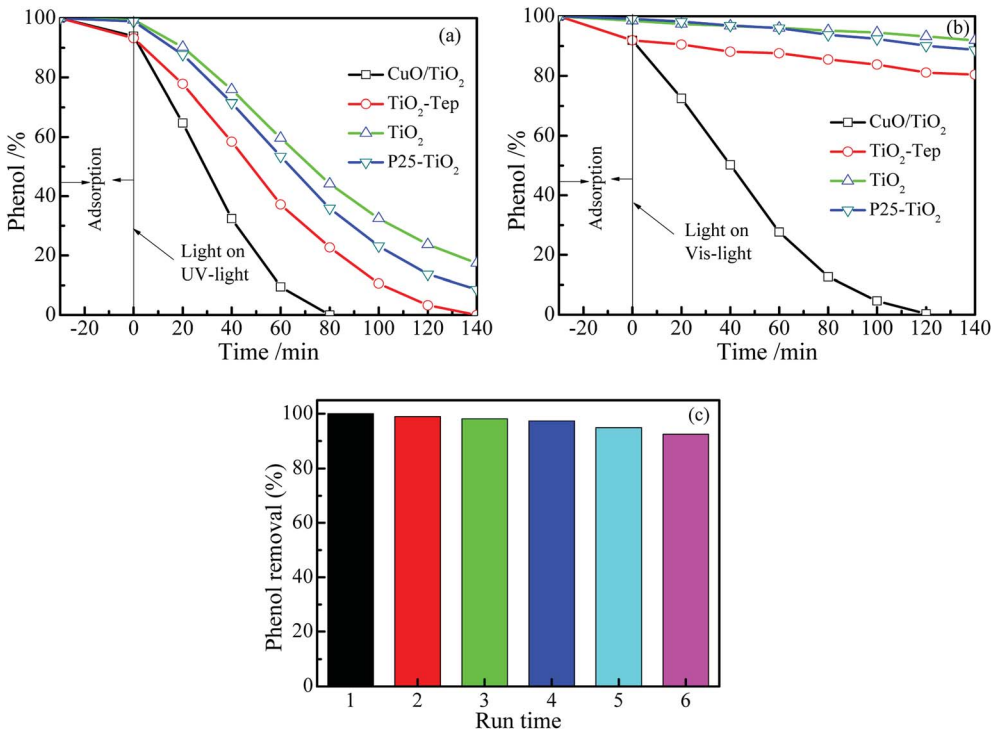

Fig. 6 Phenol photocatalytic degradation over CuO/TiO_2, TiO_2-Tep, TiO_2, and P25-TiO_2 under (a) UV and (b) visible light. (c) The reusability of CuO/TiO_2 for phenol degradation under visible light.

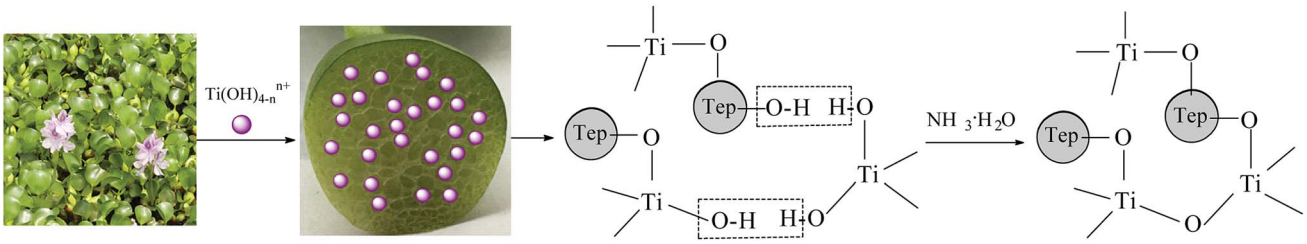

Fig. 7 The proposed mechanism for the synthesis of TiO_2 with *Eichhornia crassipes* template.

The following mechanism is proposed for the synthesis of TiO_2 with *Eichhornia crassipes* template. When the $TiCl_4$ is added into the *Eichhornia crassipes* suspension, hydrolyzed products of $Ti(OH)_{4-n}^{n+}$ are obtained (equn (1)).[40] Then, the $Ti(OH)_{4-n}^{n+}$ rapidly disperses through the mesh in *Eichhornia crassipes* and attaches to the mesh wall (Fig. 7). $Ti(OH)_{4-n}^{n+}$ interacts with the hydroxy group on the surface of the template and further hydrolyzes to form the nucleation O_nTi–(O-template)$_{4-n}$ (eqn (2)). After addition of $NH_3 \cdot H_2O$, template-TiO_2 (eqn (3)) is formed. During the reaction process, the growth of TiO_2 is blocked by the three-dimensional network structure of *Eichhornia crassipes*, the hydroxyl group of the *Eichhornia crassipes* combines with the hydroxy group of TiO_2 (Fig. 7), and crystalline growth and grain agglomeration of the TiO_2 precursor are inhibited.[40,42] Finally, the template is removed by calcination, leaving CuO/TiO_2.

$$TiCl_4 + (4-n)H_2O \rightleftharpoons Ti(OH)_{4-n}^{n+} + (4-n)H^+ + 4Cl^- \quad (1)$$

$$Ti(OH)_{4-n}^{n+} + (4-n)\text{Template-OH} \rightleftharpoons O_nTi - (-\text{O-Template})_{4-n} + (4-n)H^+ \quad (2)$$

$$O_nTi - (-\text{O-Template})_{4-n} \xrightleftharpoons{NH_3 \cdot H_2O} \text{Template-}TiO_2 \quad (3)$$

4. Conclusions

A CuO/TiO_2 composite photocatalyst was prepared by a facile hydrolysis method using the aquatic plant *Eichhornia crassipes* as a template. The CuO/TiO_2 catalyst had excellent catalytic activity for the removal of phenol under UV and visible light irradiation. Phenol was completely removed by CuO/TiO_2 in 80 min and 120 min under UV and visible light sources, respectively. The CuO/TiO_2 synthesized with the *Eichhornia crassipes* template was effective for degradation of phenol. The catalytic efficiency of the CuO/TiO_2 catalyst may be due to the porosity of the material, which is governed by the three-dimensional network structure and the hydroxyl functional group of the *Eichhornia crassipes* in the synthetic process. The *Eichhornia crassipes* also prevents the crystal growth and aggregation and enhances the catalytic activity. Moreover, the formation of a p–n CuO/TiO_2 heterojunction facilitates the separation of photogenerated electrons and holes and improves the photocatalytic activity of the material.

Conflicts of interest

There are no conflicts to declare.

Acknowledgements

This work was supported by the National Natural Science Foundation of China under the Grant No. 31000269, China Postdoctoral Program under the grant No. 2018M632562, and Strait Postdoctoral Program under the grant No. 1323H0005.

References

1 M. Wang, L. Sun, Z. Lin, J. Cai, K. Xie and C. Lin, *Energy Environ. Sci.*, 2013, **6**, 1211.
2 X. Hu, Q. Zhu, X. Wang, N. Kawazoe and Y. Yang, *J. Mater. Chem. A*, 2015, **3**, 17858–17865.
3 Y.-T. Liao, C.-W. Huang, C.-H. Liao, J. C. S. Wu and K. C. W. Wu, *Appl. Energy*, 2012, **100**, 75–80.
4 Z. Zhang, X. Jiang, B. Liu, L. Guo, N. Lu, L. Wang, J. Huang, K. Liu and B. Dong, *Adv. Mater.*, 2018, **30**, 1705221.
5 Z. Zhang, Y. Liu, Y. Fang, B. Cao, J. Huang, K. Liu and B. Dong, *Adv. Sci.*, 2018, **5**, 1800748.
6 N. Lu, Z. Zhang, Y. Wang, B. Liu, L. Guo, L. Wang, J. Huang, K. Liu and B. Dong, *Appl. Catal., B*, 2018, **233**, 19–25.
7 Z. Zhang, J. Huang, Y. Fang, M. Zhang, K. Liu and B. Dong, *Adv. Mater.*, 2017, **29**, 1606688.
8 B. Khezri, A. C. Fisher and M. Pumera, *J. Mater. Chem. A*, 2017, **5**, 8230–8246.
9 W.-c. Peng, X. Wang and X.-y. Li, *Nanoscale*, 2014, **6**, 8311.
10 H.-W. Chen, C.-Y. Hong, C.-W. Kung, C.-Y. Mou, K. C. W. Wu and K.-C. Ho, *J. Power Sources*, 2015, **288**, 221–228.
11 B. Lai, Y. Zhang, Z. Chen, P. Yang, Y. Zhou and J. Wang, *Appl. Catal., B*, 2014, **144**, 816–830.
12 H. M. Saleh, T. A. Bayoumi, H. H. Mahmoud and R. F. Aglan, *Nucl. Eng. Des.*, 2017, **315**, 194–199.
13 P. J. C. Favas, J. Pratas and M. N. V. Prasad, *Sci. Total Environ.*, 2012, **433**, 390–397.
14 C. Yu, Z. Wu, R. Liu, D. D. Dionysiou, K. Yang, C. Wang and H. Liu, *Appl. Catal., B*, 2017, **209**, 1–11.
15 H. He, B. Huang, G. Fu, Y. Du, D. Xiong, C. Lai and X. Pan, *J. Hazard. Mater.*, 2017, **340**, 120–129.
16 I. Zinicovscaia, in *Cyanobacteria for Bioremediation of Wastewaters*, ed. I. Zinicovscaia and L. Cepoi, Springer International Publishing, Cham, 2016, pp. 17–25, DOI: 10.1007/978-3-319-26751-7_3.

17 C. A. Martínez-Huitle and E. Brillas, *Appl. Catal., B*, 2009, **87**, 105–145.
18 D. P. Zagklis, P. G. Koutsoukos and C. A. Paraskeva, *Ind. Eng. Chem. Res.*, 2012, **51**, 15456–15462.
19 A. Ajmal, I. Majeed, R. N. Malik, M. Iqbal, M. A. Nadeem, I. Hussain, S. Yousaf, G. Zeshan, G. Mustafa, M. I. Zafar and M. A. Nadeem, *J. Environ. Chem. Eng.*, 2016, **4**, 2138–2146.
20 J. E. Chen, H.-Y. Lian, S. Dutta, S. M. Alshehri, Y. Yamauchi, M. T. Nguyen, T. Yonezawa and K. C. W. Wu, *Phys. Chem. Chem. Phys.*, 2015, **17**, 27653–27657.
21 Z. Zhang, J. Huang, M. Zhang, Q. Yuan and B. Dong, *Appl. Catal., B*, 2015, **163**, 298–305.
22 X. Xu, X. Fang, T. Zhai, H. Zeng, B. Liu, X. Hu, Y. Bando and D. Golberg, *Small*, 2011, **7**, 445–449.
23 O. A. Zelekew, D.-H. Kuo, J. M. Yassin, K. E. Ahmed and H. Abdullah, *Appl. Surf. Sci.*, 2017, **410**, 454–463.
24 S. Naraginti, F. B. Stephen, A. Radhakrishnan and A. Sivakumar, *Spectrochim. Acta, Part A*, 2015, **135**, 814–819.
25 N. Wei, H. Cui, Q. Song, L. Zhang, X. Song, K. Wang, Y. Zhang, J. Li, J. Wen and J. Tian, *Appl. Catal., B*, 2016, **198**, 83–90.
26 B. Jiang, L. Jiang, X. Shi, W. Wang, G. Li, F. Zhu and D. Zhang, *J. Sol-Gel Sci. Technol.*, 2014, **73**, 314–321.
27 M. Daous, V. Iliev and L. Petrov, *J. Mol. Catal. A: Chem.*, 2014, **392**, 194–201.
28 Y. Yu, Y. Tang, J. Yuan, Q. Wu, W. Zheng and Y. Cao, *J. Phys. Chem. C*, 2014, **118**, 13545–13551.
29 J. Bandara, C. P. K. Udawatta and C. S. K. Rajapakse, *Photochem. Photobiol. Sci.*, 2005, **4**, 857–861.
30 E. Ovodok, H. Maltanava, S. Poznyak, M. Ivanovskaya, A. Kudlash, N. Scharnagl and J. Tedim, *Mater. Today Proc.*, 2017, **4**, 11526–11533.
31 X. Yang, H. Fu, A. Yu and X. Jiang, *J. Colloid Interface Sci.*, 2012, **387**, 74–83.
32 Y.-T. Liao, Y.-Y. Huang, H. M. Chen, K. Komaguchi, C.-H. Hou, J. Henzie, Y. Yamauchi, Y. Ide and K. C. W. Wu, *ACS Appl. Mater. Interfaces*, 2017, **9**, 42425–42429.
33 J. L. Vivero-Escoto, Y.-D. Chiang, K. Wu and Y. Yamauchi, *Sci. Technol. Adv. Mater.*, 2012, **13**, 013003.
34 J. C. Colmenares, R. S. Varma and P. Lisowski, *Green Chem.*, 2016, **18**, 5736–5750.
35 M. A. Mohamed, W. N. W. Salleh, J. Jaafar, Z. A. Mohd Hir, M. S. Rosmi, M. A. Mutalib, A. F. Ismail and M. Tanemura, *Carbohydr. Polym.*, 2016, **146**, 166–173.
36 B. A. Marinho, R. O. Cristóvão, R. Djellabi, J. M. Loureiro, R. A. R. Boaventura and V. J. P. Vilar, *Appl. Catal., B*, 2017, **203**, 18–30.
37 S. Rezania, S. M. Taib, M. F. Md Din, F. A. Dahalan and H. Kamyab, *J. Hazard. Mater.*, 2016, **318**, 587–599.
38 B. Lu, Z. Xu, J. Li and X. Chai, *Ecol. Eng.*, 2018, **110**, 18–26.
39 I. Panfili, M. L. Bartucca, E. Ballerini and D. Del Buono, *Sci. Total Environ.*, 2017, **601–602**, 1263–1270.
40 X. Chen, D.-H. Kuo, D. Lu, Y. Hou and Y.-R. Kuo, *Microporous Mesoporous Mater.*, 2016, **223**, 145–151.
41 X. Chen, D.-H. Kuo and D. Lu, *Chem. Eng. J.*, 2016, **295**, 192–200.
42 Y. Zhou, E.-Y. Ding and W.-D. Li, *Mater. Lett.*, 2007, **61**, 5050–5052.
43 S. Miao, Z. Miao, Z. Liu, B. Han, H. Zhang and J. Zhang, *Microporous Mesoporous Mater.*, 2006, **95**, 26–30.
44 X. Li, T. Fan, H. Zhou, S.-K. Chow, W. Zhang, D. Zhang, Q. Guo and H. Ogawa, *Adv. Funct. Mater.*, 2009, **19**, 45–56.
45 X. Shari Li, G. E. Fryxell, C. Wang and J. Young, *Inorg. Chem. Commun.*, 2006, **9**, 7–9.
46 X. Chen and D.-H. Kuo, *ACS Sustainable Chem. Eng.*, 2017, **5**, 4133–4143.
47 X. Chen, D.-H. Kuo, A. D. Saragih, Z.-Y. Wu, H. Abdullah and J. Lin, *Chem. Eng. Sci.*, 2019, **194**, 105–115.
48 L. S. G. Y. N. Z. C. Mingqing, *Chin. J. Mater. Res.*, 2010, **24**, 610–614.
49 X. Chen and S. S. Mao, *Chem. Rev.*, 2007, **107**, 2891–2959.
50 J. Low, B. Cheng and J. Yu, *Appl. Surf. Sci.*, 2017, **392**, 658–686.
51 S. Ma, J. Xue, Y. Zhou and Z. Zhang, *J. Mater. Chem. A*, 2014, **2**, 7272–7280.
52 O. Ahmed Zelekew and D.-H. Kuo, *Phys. Chem. Chem. Phys.*, 2016, **18**, 4405–4414.